

Resolution-Adaptive Micro-Doppler Spectrogram for Human Activity Recognition

Do-Hyun Park, *Graduate Student Member, IEEE*, Min-Wook Jeon, *Graduate Student Member, IEEE*,
and Hyoung-Nam Kim, *Member, IEEE*

Abstract—The rising demand for remote-sensing systems for detecting hazardous situations has led to increased interest in radar-based human activity recognition (HAR). Conventional radar-based HAR methods predominantly rely on micro-Doppler spectrograms for recognition tasks. However, spectrograms frequently fail to effectively capture micro-Doppler signatures because of their limited linear resolution. To address this limitation, we propose a time–frequency domain representation method that adaptively adjusts the resolution based on activity characteristics. This approach nonlinearly transforms the resolution to focus on the most relevant frequency range for micro-Doppler signatures. We validate the proposed method by training deep-learning-based HAR models on datasets generated using the adaptive representation method. Experimental results demonstrate that the models trained using the proposed method achieve superior recognition accuracy compared with those trained using conventional methods.

Index Terms—human activity recognition, micro-Doppler, pattern analysis, machine learning

I. INTRODUCTION

Recent radar systems have been actively utilized in various fields, including tracking moving individuals [1], recognizing hand gestures [2], and monitoring vital signs [3], [4]. The demand for elderly care and healthcare is rising owing to an increase in the aging population. This emphasizes the importance of radar-based human activity recognition (HAR) systems that can detect dangerous situations such as falls [5], [6]. Radar-based HAR systems recognize human activities by analyzing the micro-Doppler effect embedded in target-echo signals. The micro-Doppler effect represents the frequency shifts caused by the minute movements of a target, and it serves as a key feature for identifying various human activities.

HAR systems employ signal processing techniques that appropriately represent received signals to effectively capture the movements of different body parts. Signals are primarily transformed into two-dimensional data using various preprocessing methods. For instance, the data received by a radar system can be represented in the Doppler-time domain (also known as a spectrogram) [7], [8], range-time domain [9], or range-Doppler domain [10]. Despite these diverse approaches, numerous studies still utilize spectrograms for HAR systems because they effectively capture the movement characteristics of different body parts [11].

The accuracy of spectrogram-based HAR systems can be strongly influenced by the time–frequency domain representation methods of received radar signals. Current time–frequency analysis methods employed in HAR systems can be broadly classified into two categories: linear and quadratic time–frequency analyses. Linear time–frequency analysis typically involves a short-time Fourier transform (STFT). In the STFT, the time-domain signal is divided into fixed intervals, and a Fourier transform is performed on each segment to obtain time–frequency domain information. However, the fixed-length window function used in the STFT results in a trade-off between the time and frequency resolution. Quadratic time–frequency analysis includes methods such as the Wigner–Ville distribution (WVD), smoothed pseudo WVD (SPWVD), and reduced interference distribution using the Hanning kernel (RIDHK). Although the WVD provides a high time–frequency resolution, it experiences cross-term interference problems. SPWVD is an advanced method derived from WVD, and it effectively suppresses cross-term interference while maintaining a high time–frequency resolution, thereby allowing for accurate signal feature representation. The RIDHK provides a higher time–frequency resolution compared with the SPWVD but with increased cross-term interference. As each of these techniques provides diverse advantages, ongoing research has explored the use of the SPWVD and RIDHK in HAR applications [7], [12], [13].

The aforementioned time–frequency representation methods are useful for visualizing various micro-Doppler signatures. However, they have limitations in analyzing subtle patterns associated with human activities. Existing time–frequency analysis methods, which use fixed window sizes, exhibit a linearly distributed resolution for time and frequency. This makes it challenging to capture detailed features from the micro-Doppler effects caused by fine movements such as the vibration or rotation of body parts. To address these limitations, this study proposes a time–frequency representation technique that is optimized for analyzing distinctive micro-Doppler signature patterns associated with human activities. The proposed method adaptively adjusts the frequency-domain resolution, thus allowing for the accurate capture of micro-Doppler signatures generated by human movements. We use experimental data to validate the superiority of the proposed method by comparing the recognition performance of deep learning models trained on datasets generated using conventional time–frequency analysis techniques with those generated using the proposed technique. This comparison demonstrates the effectiveness of the proposed method in improving the

Do-Hyun Park and Min-Wook Jeon are with the Department of Electrical and Electronics Engineering, Pusan National University, Busan 46241, Republic of Korea.

Hyoung-Nam Kim is with the School of Electrical and Electronics Engineering, Pusan National University, Busan 46241, Republic of Korea.

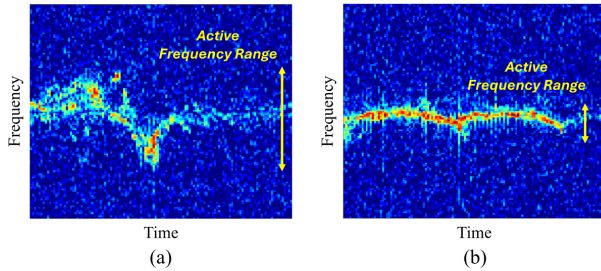


Fig. 1. Examples of spectrograms showing distinct micro-Doppler signatures obtained from various human activities: (a) falling, (b) limping.

HAR accuracy.

The rest of this letter is organized as follows: Section II describes the preprocessing technique for frequency-modulated continuous-wave (FMCW) radar and the method for generating spectrograms. Section III introduces the proposed spectrogram generation method with adaptive resolution. In Section IV, we present the performance analysis results obtained using real-world data and compare the recognition performance with those of existing methods. Finally, Section V concludes the letter.

II. PREPROCESSING FOR FMCW RADAR-BASED HAR

FMCW radar-based HAR systems perform a preprocessing step to extract features related to fine human movements from raw radar signals. First, the received raw data are arranged into a two-dimensional data matrix. Here, one axis represents the fast time, which corresponds to the time per sweep, and the other axis represents the slow time, which indicates the index of chirps over the measurement duration. Then, a Fourier transform is applied to the fast time domain to yield $\mathbf{x}(r, n)$, which contains the magnitude of the r -th range bin at the n -th chirp [14]. The distance information proportional to the delay time of the target echo can be extracted from $\mathbf{x}(r, n)$ [15]. A 4th-order high-pass Butterworth notch filter with a cutoff frequency of 0.01 Hz is applied to $\mathbf{x}(r, n)$ to remove static clutter.

Time–frequency analysis is performed in the slow time domain of filtered $\mathbf{x}(r, n)$ to generate a spectrogram composed of time and frequency domains, thereby allowing for the visualization of micro-Doppler signatures. The spectrogram, $\text{SPEC}(t, f)$, can be obtained using the STFT, as follows:

$$\text{SPEC}(t, f) = \left| \sum_n \sum_{r=r_s}^{r_e} \mathbf{x}(r, n) w(n-t) e^{-j2\pi f n} \right|^2, \quad (1)$$

where r_s and r_e represent the start and end range bins for the analysis, respectively, and $w(\cdot)$ denotes the window function.

Fig. 1 presents the examples of spectrograms generated from signals containing micro-Doppler effects caused by various human activities. Different human movements generate unique micro-Doppler signatures, which are clearly visible in the spectrograms. However, the fixed time and frequency resolution of the STFT poses a limitation in optimizing the analysis of micro-Doppler signatures associated with diverse human activities. This limitation is due to the varying frequency

ranges generated by different actions. For instance, as shown in Fig. 1(a), a falling action results in a micro-Doppler signature distributed across a wide frequency range, making it relatively straightforward to observe. In contrast, the limping movement shown in Fig. 1(b) exhibits a narrower frequency range, making the features within its micro-Doppler signature less prominent.

III. RESOLUTION-ADAPTIVE SPECTROGRAM

This study proposes a spectrogram transformation method to increase the precision of micro-Doppler signature analysis and address the limitations of conventional spectrograms. The proposed technique consists of two steps: (1) identifying the frequency range of micro-Doppler signatures; and (2) nonlinearly adjusting the frequency-domain resolution according to the identified range. This allows for accurate feature analysis that is customized for the characteristics of each micro-Doppler signature.

To adaptively adjust the resolution, Algorithm 1 transforms the conventional spectrogram into a resolution-adaptive (RA) spectrogram, $\text{SPEC}_{\text{RA}}(t, m)$. The inputs for this algorithm are the spectrogram, $\text{SPEC}(t, f)$, number of filters in the filter bank, M , and the maximum frequency of the spectrogram, f_{max} . In the first step, the spectrogram undergoes a log transformation and is then projected onto the time domain to create $e(f)$, which represents the energy distribution across frequencies. This helps clearly identify the energy distribution of the micro-Doppler signatures in the frequency domain.

To explore the active frequency range corresponding to different activities, the negative corner frequency, f_{nc} , and positive corner frequency f_{pc} , are determined as the values of f_1 and f_2 that minimize $J(f_1, f_2)$, respectively. $J(f_1, f_2)$ is expressed as follows:

$$J(f_1, f_2) = \text{LogMS}(-f_{\text{max}}, f_1) + \text{LogMS}(f_1, f_2) + \text{LogMS}(f_2, f_{\text{max}}), \quad (2)$$

where $\text{LogMS}(\cdot)$ represents the logarithmic mean square, which is defined as

$$\text{LogMS}(n, m) = (m - n + 1) \log \left(\frac{1}{m - n + 1} \sum_{i=n}^m e^2(i) \right). \quad (3)$$

To maintain the stability of the resolution adjustment, the corner frequency, f_c , is selected as the larger value between $|f_{nc}|$ and f_{pc} .

As a part of the nonlinear frequency transformation, the linear frequency points from the spectrogram are mapped to their corresponding positions on the nonlinear frequency scale. The scaling function that transforms the linear frequency component, f , into the nonlinear frequency scale, $S(f)$, is defined as follows:

$$S(f) = \frac{f_c}{\log(2)} \log \left(1 + \frac{f}{f_c} \right). \quad (4)$$

The scaling function described in (4) is applied to densely analyze the frequency range below f_c at an approximately linear scale, thereby providing a higher resolution. In contrast, the

Algorithm 1: Frequency resolution-adaptive spectrogram generation

Input : $\text{SPEC}(t, f)$, M , f_{\max}
Output: $\text{SPEC}_{\text{RA}}(t, m)$

- 1 $e(f) \leftarrow \sum_t \log(\text{SPEC}(t, f))$
- 2 $f_{nc}, f_{pc} \leftarrow \min_{f_1, f_2} J(f_1, f_2)$
- 3 $f_c \leftarrow \max(|f_{nc}|, f_{pc})$
- 4 Calculate $S(f_{\max})$ using (4)
- 5 Compute P_m for $m = 0, 1, \dots, M + 1$ as evenly spaced points between 0 and $S(f_{\max})$
- 6 Convert P_m to p_m using (5)
- 7 **for** iteration $m = 1, \dots, M$ **do**
- 8 **for** iteration $f = 0, \dots, f_{\max}$ **do**
- 9 Compute m -th filter $\text{FB}(m, f)$ using (6)
- 10 **end**
- 11 **end**
- 12 $\text{SPEC}_{\text{pos}}(t, m) \leftarrow \sum_{f=0}^{f_{\max}} \text{FB}(m, f) \cdot \text{SPEC}(t, f)$
- 13 $\text{SPEC}_{\text{neg}}(t, m) \leftarrow \sum_{f=0}^{f_{\max}} \text{FB}(m, f) \cdot \text{SPEC}(t, -f)$
- 14 Construct $\text{SPEC}_{\text{RA}}(t, m)$ by combining $\text{SPEC}_{\text{pos}}(t, m)$ and $\text{SPEC}_{\text{neg}}(t, m)$

frequency range above f_c is sparsely analyzed at a nonlinear scale, resulting in a lower resolution.

After $S(f_{\max})$ is computed with the scaling function, nonlinear frequency points, P_m , are generated with $M + 2$ uniformly distributed points between 0 and $S(f_{\max})$. Points P_m are mapped back to their corresponding linear frequency points, p_m , by applying the following inverse transformation:

$$p_m = f_c \cdot (10^z - 1),$$

$$z = \frac{\log(2) \cdot P_m}{f_c}. \quad (5)$$

To facilitate resolution adjustment using p_m , the filter bank, $\text{FB}(m, f)$, is derived as follows:

$$\text{FB}(m, f) = \begin{cases} \frac{f - p_{m-1}}{p_m - p_{m-1}}, & \text{if } p_{m-1} \leq f \leq p_m \\ \frac{p_{m+1} - f}{p_{m+1} - p_m}, & \text{if } p_m < f \leq p_{m+1} \\ 0, & \text{otherwise} \end{cases} \quad (6)$$

The filters in the filter bank are designed such that for each frequency point, they linearly increase from 0 to 1 between the previous and current frequency points and linearly decrease from 1 to 0 between the current and subsequent frequency points. This filter bank is independently applied to the positive and negative frequency components of the spectrogram. The processed positive and negative frequency components are then recombined to generate the RA spectrogram.

Figs. 2 and 3 illustrate the process and results of generating RA spectrograms using the proposed method for various activities. Fig. 2 presents the results of identifying the negative and positive corner frequencies for the falling and limping motions. The corner frequency is subsequently employed to adjust the spectrogram resolution. The examples of the RA spectrogram shown in Fig. 3 illustrate that the enhanced

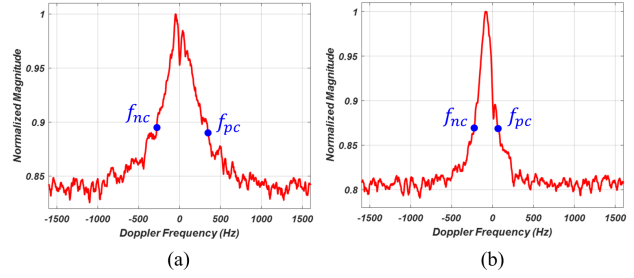


Fig. 2. Examples of $e(f)$ and corner frequency results for various activities: (a) falling, (b) limping.

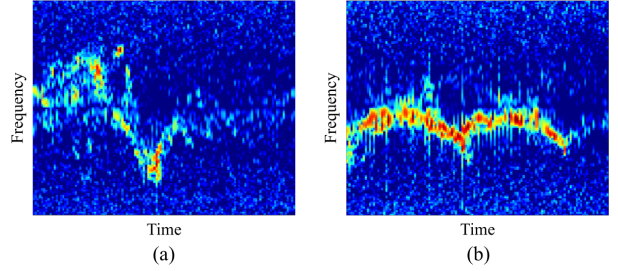


Fig. 3. Examples of RA spectrograms generated from various human activities: (a) falling, (b) limping.

resolution within the frequency range corresponding to micro-Doppler signatures allows for precise pattern analysis.

Fig. 4 presents the tracking results of micro-Doppler signatures in the conventional and RA spectrograms, which highlight the extent of resolution improvement. Signature tracking is performed by extracting the frequency index with the highest value for each time index within each spectrogram, followed by the application of a Kalman filter. This comparison demonstrates that the resolution enhancement in the RA spectrogram significantly contributes to a more accurate analysis of micro-Doppler signature features. It should be noted that in Figs. 3(b) and 4(b), the improved resolution substantially enhances the clarity of signature features for activities such as limping, which are primarily concentrated in the low-frequency band. These findings demonstrate the strong impact of resolution enhancement in such cases.

IV. PERFORMANCE ANALYSIS

We collected data for various daily activities to evaluate the performance of the proposed method. The data were acquired using the Texas Instruments AWR1642BOOST FMCW radar. Participants performed six different daily activities (A1 to A6: falling, limping, picking up objects, running, sitting, and walking) within a range of 4 m with respect to the radar. To ensure the diversity of the dataset, five participants (P1 to P5) contributed to the data collection process, resulting in 2,250 activity data samples. The data obtained from four participants were utilized to train the deep-learning-based recognition model. The data obtained from one participant, which were not included in the training dataset, were used for testing. This approach ensured an unbiased assessment of the generalization capability of the model.

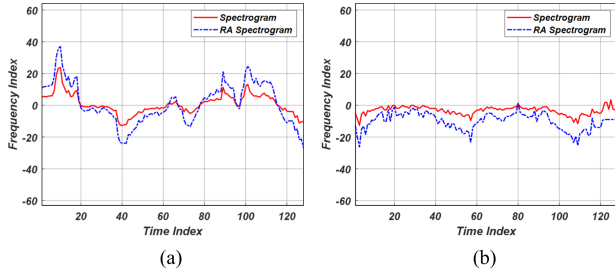


Fig. 4. Examples of micro-Doppler signature tracking results for various activities: (a) falling, (b) limping.

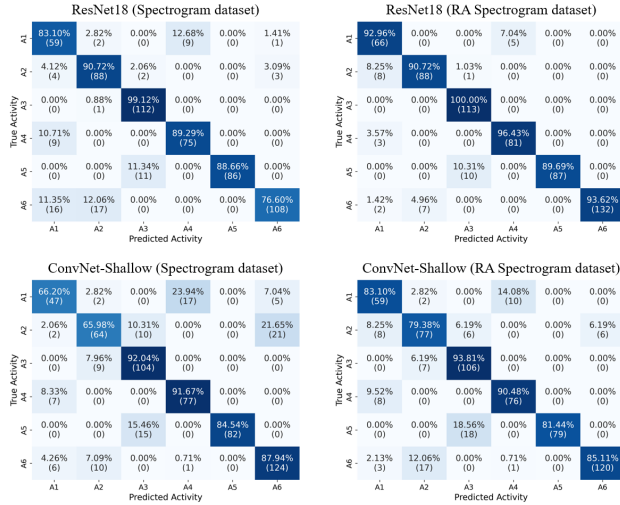


Fig. 5. Confusion matrices for models trained on conventional and RA spectrogram datasets.

We compared the recognition performances of HAR models trained on datasets obtained using conventional time–frequency analysis methods with those trained on datasets obtained using the proposed method. The RA spectrogram was generated using MATLAB code, which is freely available in the GitHub repository¹. The input image data were log-transformed and preprocessed by normalizing them to have a mean of 0 and variance of 1. This enabled the models to effectively analyze the features presented in the time–frequency images. For the HAR models, we utilized convolutional neural network (CNN) models that were previously used in HAR research [16], [17]. In addition, we utilized CNN models that are widely used in image classification, such as ResNet18 [18], VGG16, and VGG19 [19].

Fig. 5 presents the confusion matrices that compare actual activities with those predicted by the HAR model. The ResNet18 and ConvNet-Shallow models were used with datasets constructed using conventional and proposed RA spectrograms. The training datasets consisted of P2–P5 data, whereas the test dataset consisted of P1 data. The comparative results show that the models trained on RA spectrograms achieve a higher average recognition accuracy than those trained on conventional spectrograms. In particular, there is a marked improvement in the recognition accuracy of the A1

TABLE I
ACCURACY OF HAR MODELS FOR DATASETS USING P1 TEST DATA

Model	Recognition Accuracy			
	Spectrogram	SPWVD	RIDHK	RA Spectrogram
CNN [16]	88.39	86.40	86.40	91.87
ConvNet-Deep [17]	90.88	89.72	91.38	94.69
ConvNet-Shallow [17]	82.59	77.78	77.61	85.74
ResNet18 [18]	87.56	92.37	88.89	94.03
VGG16 [19]	89.88	89.55	91.38	93.86
VGG19 [19]	89.39	88.72	88.06	93.70

TABLE II
ACCURACY OF HAR MODELS FOR DATASETS USING P2 TEST DATA

Model	Recognition Accuracy			
	Spectrogram	SPWVD	RIDHK	RA Spectrogram
CNN [16]	95.39	93.57	93.41	96.87
ConvNet-Deep [17]	96.54	95.39	94.40	97.69
ConvNet-Shallow [17]	77.92	75.29	81.55	86.33
ResNet18 [18]	90.28	92.75	94.23	97.03
VGG16 [19]	93.74	93.41	93.25	95.39
VGG19 [19]	92.09	90.94	94.73	94.56

activity (falling), which is a critical factor in HAR because of its significance in safety and health monitoring applications.

Tables I and II present the average recognition accuracies for the models based on various time–frequency analysis methods. In most cases, the models that use the proposed RA spectrogram demonstrate the highest recognition accuracy. It should be noted that for the P1 test dataset, the VGG19 model achieves a recognition accuracy of 93.7% when the RA spectrogram dataset is used. This represents an improvement of 4.31%–5.64% over the same model with other time–frequency representation methods. Similarly, for the P2 test dataset, the ConvNet-Shallow model achieves an accuracy of 86.33% with the RA spectrogram, which exceeds the accuracy of other preprocessing methods by 4.78%–11.04%. These results demonstrate that the RA spectrogram provides a refined resolution that is suitable for human activity analysis. The proposed method more effectively captures and classifies micro-Doppler signature patterns compared with existing methods.

V. CONCLUSION

We propose a time–frequency representation method that adaptively adjusts the resolution. The proposed method explores the frequency range of micro-Doppler signatures within a spectrogram and applies a nonlinear transformation to the frequency resolution within the identified range. Experimental results demonstrate that the proposed approach achieves a higher recognition accuracy compared with various time–frequency analysis techniques. Although this study focuses on environments in which a single activity is performed during the measurement time, continuous HAR systems may encounter idle times with no activity in the time domain. Therefore, future work will focus on enhancing the HAR system by developing methods that simultaneously adapt the resolution in the time and frequency domains.

¹<https://github.com/Signal-Park/Resolution-Adaptive-Spectrogram>

REFERENCES

- [1] Y. He, P. Aubry, F. L. Chevalier, and A. Yarovoy, "Decentralised tracking for human target in multistatic ultra-wideband radar," *IET Radar, Sonar & Navigation*, vol. 8, no. 9, pp. 1215-1223, Dec. 2014.
- [2] Y. Kim and B. Toomajian, "Hand Gesture Recognition Using Micro-Doppler Signatures With Convolutional Neural Network," *IEEE Access*, vol. 4, pp. 7125-7130, 2016.
- [3] C. Li, V. M. Lubecke, O. Boric-Lubecke, and J. Lin, "A Review on Recent Advances in Doppler Radar Sensors for Noncontact Healthcare Monitoring," *IEEE Trans. Microw. Theory Tech.*, vol. 61, no. 5, pp. 2046-2060, May 2013.
- [4] M. Alizadeh, G. Shaker, J. C. M. D. Almeida, P. P. Morita, and S. Safavi-Naeini, "Remote Monitoring of Human Vital Signs Using mm-Wave FMCW Radar," *IEEE Access*, vol. 7, pp. 54958-54968, 2019.
- [5] M. G. Amin, Y. D. Zhang, F. Ahmad, and K. C. D. Ho, "Radar signal processing for elderly fall detection: The future for in-home monitoring," *IEEE Signal Process. Mag.*, vol. 33, no. 2, pp. 71-80, Mar. 2016
- [6] I. Ullmann, R. G. Guendel, N. C. Kruse, F. Fioranelli, and A. Yarovoy, "A Survey on Radar-Based Continuous Human Activity Recognition," *IEEE J. Microw.*, vol. 3, no. 3, pp. 938-950, Jul. 2023.
- [7] L. Tang, Y. Jia, Y. Qian, S. Yi, and P. Yuan, "Human Activity Recognition Based on Mixed CNN With Radar Multi-Spectrogram," *IEEE Sens. J.*, vol. 21, no. 22, pp. 25950-25962, Nov. 2021.
- [8] Y. Yang, Y. Zhang, H. Ji, B. Li and C. Song, "Radar-Based Human Activity Recognition Under the Limited Measurement Data Support Using Domain Translation," in *IEEE Signal Process. Lett.*, vol. 29, pp. 1993-1997, Sep. 2022.
- [9] R. G. Guendel, F. Fioranelli, and A. Yarovoy, "Derivative Target Line (DTL) for Continuous Human Activity Detection and Recognition," *2020 IEEE Radar Conf. (RadarConf20)*, Florence, Italy, 2020, pp. 1-6.
- [10] C. Ding et al., "Continuous human motion recognition with a dynamic range-Doppler trajectory method based on FMCW radar," *IEEE Trans. Geosci. Remote Sens.*, vol. 57, no. 9, pp. 6821-6831, Sep. 2019.
- [11] S. Zhu, R. G. Guendel, A. Yarovoy, and F. Fioranelli, "Continuous Human Activity Recognition With Distributed Radar Sensor Networks and CNN-RNN Architectures," *IEEE Trans. Geosci. Remote Sens.*, vol. 60, Art no. 5115215, Jul. 2022.
- [12] Z. Liu, L. Xu, Y. Jia, and S. Guo, "Human Activity Recognition Based on Deep Learning with Multi-spectrogram," *2020 IEEE 5th Int. Conf. on Signal and Image Proc. (ICSIP)*, Nanjing, China, 2020, pp. 11-15.
- [13] Y. Qian, C. Chen, L. Tang, Y. Jia, and G. Cui, "Parallel LSTM-CNN Network With Radar Multispectrogram for Human Activity Recognition," *IEEE Sens. J.*, vol. 23, no. 2, pp. 1308-1317, Jan. 2023.
- [14] X. Li, Z. Li, F. Fioranelli, S. Yang, O. Romain, J. L. Kerneç, "Hierarchical Radar Data Analysis for Activity and Personnel Recognition," *Remote Sen.*, vol. 12, no. 14, 2237, 2020.
- [15] W. -Y. Kim and D. -H. Seo, "Radar-Based Human Activity Recognition Combining Range-Time-Doppler Maps and Range-Distributed-Convolutional Neural Networks," *IEEE Trans. Geosci. Remote Sens.*, vol. 60, Art no. 1002311, Mar. 2022.
- [16] T. S. Jordan, "Using convolutional neural networks for human activity classification on micro-Doppler radar spectrograms." *SPIE DEFENSE + SECURITY*, vol. 9825, no. 9, May 2016.
- [17] X. Yang, R. G. Guendel, A. Yarovoy, and F. Fioranelli, "Radar-based Human Activities Classification with Complex-valued Neural Networks," *2022 IEEE Radar Conf. (RadarConf22)*, New York City, NY, USA, 2022, pp. 1-6.
- [18] K. He, X. Zhang, S. Ren, and J. Sun, "Deep residual learning for image recognition," *Proc. IEEE Conf. Comput. Vis. Pattern. Recognit.*, Las Vegas, NV, USA, Jun. 2016, pp. 770-778.
- [19] K. Simonyan and A. Zisserman, "Very Deep Convolutional Networks for Large-Scale Image Recognition," *3rd Int. Conf. Learn. Represent.*, San Diego, CA, USA, May 2015, pp. 1-4.